

**IN-VIVO VALIDATION OF A NEW TECHNIQUE
THAT COMPENSATES FOR SOFT TISSUE
ARTEFACT IN THE UPPER-ARM: PRELIMINARY
RESULTS**

Andrea Giovanni Cutti¹, Angelo Cappello¹, Angelo Davalli²

¹ Department of Electronics, Computer Science and Systems – University of Bologna, Italy

² I.N.A.I.L. Prosthesis Centre – Vigorso di Budrio, Italy

Submitted to Clinical Biomechanics

CORRESPONDING AUTHOR

Andrea Giovanni Cutti
DEIS – University of Bologna
Viale Risorgimento, 2
I-40136 Bologna
ITALY
agcutti@deis.unibo.it
Tel: +39 051 2093904
Fax: +39 051 2093073

ABSTRACT

Background. Soft-tissue artefact is the dominant error source for upper extremity motion analyses that use skin-mounted markers, especially in humeral axial rotation. A new *in-vivo* technique has been developed to minimize this error.

Methods. This new technique is based on the definition of a humerus bone-embedded frame almost “artefact free” but influenced by the elbow orientation in the measurement of the humeral axial rotation, and on an algorithm designed to solve this kinematic coupling. The technique was validated *in-vivo* in a study of six healthy subjects who performed five arm-movement tasks. For each task the similarity between a gold standard pattern and the axial rotation pattern before and after the application of the compensation algorithm was evaluated; the similarity was assessed computing three parameters, which quantify differences in the explained variance, gain, phase and offset. In addition the *RMSE* between the patterns was used as a global similarity estimator.

Findings. Before application of the algorithm, patterns were almost uncorrelated, opposite in phase, different in gain, with a high offset and a *RMSE* averaged over the tasks of 9°. After the application, for four out of five tasks, patterns were highly correlated, in phase, with almost equal gain and limited offset; the mean *RMSE* decreased to 3°.

Interpretation. The proposed technique appears to help compensate for the soft-tissue artefact affecting axial rotation of the humerus. A further development is also proposed to make the technique effective also for the pure prono-supination task.

KEYWORDS

Movement analysis, Axial rotation, Humerus, Soft tissue artefact, Stereophotogrammetry, Calibrated Anatomical System Technique.

1. INTRODUCTION

One of the main problems with the clinical use of motion analysis systems based on skin-mounted markers is the level of accuracy of the kinematic data collected. Among the different errors identified (Leardini et al., 2005), the most significant is the so-called “soft tissue artefact” (STA), which is the displacement between markers and the underlying bone due to the interposition of active and passive soft tissues. In particular the *rigid* displacement of markers with respect to the bone was found to be the dominant component of the STA (Cappello et al., 2005), resulting in heavily corrupted estimations of joint kinematics (Cutti et al., 2005a; Lucchetti et al., 1998). To the authors’ knowledge, two STA compensation techniques were tested on upper limb movements (Roux et al., 2002; Schmidt et al., 1999) but none of them appears to be directly applicable to the upper-arm and/or for real-time applications.

The aim of this work was to develop and validate a new *in-vivo* technique to compensate for the rigid component of the STA in the upper-arm – a technique that has already been validated *in-vitro* (Cutti et al., 2005b). Since the limb movement that is most affected by the STA is the axial rotation (Cutti et al., 2005a), our study focused on the measurement accuracy of the Humerus Internal-External rotation (HIE). A key feature of this new technique is the choice of an advantageous humerus bone-embedded frame combined with a simple corrective algorithm feasible for real-time applications.

2. MATERIALS AND METHODS

2.1 DEFINITIONS OF THE HUMERUS BONE-EMBEDDED FRAME

Following the recommendations of the International Shoulder Group (ISG) (van der Helm et al., 2004), the definition of the humerus bone-embedded frame termed H2_{ISG} should be based on anatomical landmarks of the humerus and the forearm (Table 1; Table 2 - provided as on-line material); the position of these landmarks should be expressed with respect to an *upper-*

arm “cluster of markers” through a specific static-calibration trial (Fig.1a). From this definition it follows that during each given dynamic trial the pose of $H2_{ISG}$ is entirely and only linked to the upper-arm cluster and thus affected by the same STA that affects the cluster. In a recent study (Cutti et al., 2005a), the $H2_{ISG}$ measurement of HIE was found to be heavily corrupted by the STA, i.e. about 35% smaller than the real axial rotation (*HIE_r*). The in-vivo application of the ISG definition yields therefore a reliable estimate of the *HIE_r* only when the humerus is at approximately the same orientation.

FIGURE 1a,b HERE

TABLE 1 HERE

TABLE 2, ON-LINE MATERIAL, HERE

$H2_{ISG}$ definition can however be slightly modified following (Schmidt et al., 1999), in order to take into account the redundant information about the humerus pose that the forearm orientation provides during every frame of any dynamic trial. If the Ulnar Styloid (US) and the Radial Styloid (RS) are continuously used for the measurement of HIE, the new humerus bone-embedded frame $H2$ (Fig. 1b, Table 2 - provided as on-line material) becomes dependent on the forearm orientation and totally independent of the rotation of the upper-arm cluster around the long axis of the humerus: by so doing, therefore, its HIE measure (*HIE2*) becomes essentially “artefact-free”. It follows, based on this modified definition, that it *would be* possible to find a solution to the STA that affects the HIE estimation. The drawback of the above method is that *HIE2* is *kinematically coupled* with the elbow because the real axes of elbow flexion-extension and forearm pronation-supination are not generally aligned with the landmark based local coordinate systems (Veeger et al., 1997); a pure elbow flexion-extension or a pure pronation-supination movement thus generates apparent *HIE2* variations that are not related to real axial rotations, but are related to variations in the flexion-extension and

prono-supination angles of the elbow ($FLEX$, PS). On average, a pure elbow flexion-extension and prono-supination of 100° generate an apparent $HIE2$ variation of 28° and 7.5° , respectively (Cutti et al., 2005a). H2 thus represents a solution for STA that affects HIE only if the problem of its kinematic coupling with the elbow is solved. In the following sections, the kinematic coupling problem is formalized as well as the algorithm proposed for its compensation, as modified from (Cutti et al., 2005b) for this *in-vivo* application.

2.2 THE KINEMATIC COUPLING PROBLEM

Considering a generic frame i of a dynamic trial, $HIE2$ provides the actual axial rotation of the humerus $HIEr_i$ only when the elbow is flexed at 90° ($FLEX = FLEX^* = 90^\circ$) and is completely pronated ($PS = PS^*$). For other elbow orientations, $HIE2_i$ can be expressed as the sum of the real humerus internal-external rotation $HIEr_i$ and the humerus internal-external rotation error $HIEe_i$ resulting from the kinematic coupling of $HIE2_i$ with the $FLEX$ and PS values of the elbow at that frame:

$$\begin{cases} HIE2_i = HIEr_i + HIEe(FLEX_i, PS_i) \\ HIEe(FLEX^*, PS^*) = 0 \end{cases} \quad (1)$$

It follows from (1) that $HIEr_i$ can always be obtained by subtracting from the measured $HIE2_i$ the $HIEe_i$ value characteristic of the specific flexion-extension and prono-supination of the elbow at that frame:

$$HIEr_i = HIE2_i - HIEe(FLEX_i, PS_i) \quad (2)$$

Therefore, the problem of the $HIE2_i$ correction is transformed into the problem of finding an “error surface” able to provide, for every possible measured $FLEX_i$ and PS_i , the corresponding unique value of the error due to the kinematic coupling, i.e. $HIEe_i$ (Fig. 2 - supplied as on-line material).

FIGURE 2 – ON LINE MATERIAL

A limitation on the *FLEX* range considerable is in the definition of H2 itself, which becomes unreliable when the elbow is close to full extension ($FLEX < 15^\circ$) due to the fact that the long axes of the humerus and the forearm are in near alignment with each other (Schmidt et al., 1999). Considering the range of motion required to accomplish activities of the daily living (Buckley et al., 1996), only *FLEX* values greater than 30° were investigated in the study reported here.

2.3 ERROR SURFACE DETERMINATION

The error surface associated with a subject can be obtained from the subject performing a simple task, called “error surface task”, during which *HIE_r* is measurable with a good approximation. The error surface task consists of four flexion-extensions of the elbow combined with as many prono-supinations as feasible, while the subject keeps the humerus as steady as possible. In this particular, near-stationary condition of the humerus, we assume that $H2_{ISG}$ can reliably estimate the desired *HIE_r* (Cutti et al., 2005a). This assumption applied, for each frame of a trial of the “error surface task” *HIE_r*, *HIE₂*, *FLEX_i* and *PS_i* can be measured and *HIE_e* can be obtained for each frame as follows:

$$HIE_e(FLEX_i, PS_i) = HIE_2 - HIE_r \quad (3)$$

Finally, the investigated error surface, i.e. the analytical relation between *HIE_e*, *FLEX* and *PS*, can be obtained by multiple linear regression considering the entire set of frames in the trial:

$$\hat{HIE}_e = \sum_{k=0}^M a_k X_k(FLEX, PS) \quad (4)$$

where $X_k(FLEX, PS)$ are the regressors, function of the predictors $FLEX$ and PS (Petruccelli et al., 1999).

Since $HIEe$ models the kinematic coupling of $HIE2$ with the elbow, it is only dependent on the relative orientation of the forearm with respect to the humerus and not on the absolute pose of the humerus in space. In other words, the error surface obtained from an “error surface task” is one and unique for each subject and can compensate for $HIE2$ distortions during every given task of a subject *irrespective* of the absolute pose of the humerus.

2.4 COMPENSATION ALGORITHM

If the subject-specific error surface (Eq. 4) is obtained, a compensation algorithm can be constructed, based on the following procedure (Fig. 3 - supplied as on-line material): 1) calculate the orientation matrices that define the orientation $H2$ of the humerus with respect to the thorax (${}^{TH}R_{H2}^i$) and the orientation F of the forearm with respect to $H2$ (${}^{H2}R_F^i$); 2) compute $FLEX_i$, PS_i , and $HIE2_i$; 3) compute $\hat{HIE}e_i = \hat{HIE}e(FLEX_i, PS_i)$; and finally, 4) subtract $\hat{HIE}e_i$ from $HIE2_i$ to obtain the desired $HIEr_i$.

Once $HIEr_i$ is obtained, a corrected $H2$ can also be computed, and from this corrected $H2$, ${}^{H2}R_F^i$ can be re-evaluated to obtain consistent values for $FLEX$ and PS .

FIGURE 3 – NOW SUPPLIED AS ON-LINE MATERIAL.

2.5 EXPERIMENTAL SETUP

After giving their informed consent, six healthy male volunteers (average age, 35 ± 6 years; average weight, 77 ± 10 Kg; and average height, 179 ± 11 cm) were acquired using a Vicon 460 optoelectronic system (Vicon Motion Capture, Oxford, UK) with 6 video cameras.

Fourteen retro-reflective markers were placed on the thorax and on the dominant upper limb of each subject, directly on the relevant thoracic anatomical landmarks or on elastic cuffs wrapped around the humerus and forearm (Fig. 4, supplied as on-line material). The position of the upper-limb landmarks was determined through anatomical calibration (Veeger et al., 1993) as described in (Cutti et al., 2005a).

FIGURE 4 – on-line material

H_2 and $H_{2_{ISG}}$ were used to describe the humerus orientation with respect to the thorax. The forearm and thorax bone-embedded frames (Table 2 - provided as on-line material), were obtained from the ISB recommendations (van der Helm et al., 2004), assuming the ISG preferred orientation for the axes (Z axes pointing backward). The Euler angle sequence flexion-extension, ab-adduction and internal-external rotation was used to describe the kinematics of all the joints considered.

Subjects performed two groups of tasks, while always keeping the humerus as steady as possible. The first group consisted of four trials of the “error surface task”, which, considered as a single long trial, were used to compute for each subject the correspondent error surface. The second group consisted of tasks to be corrected for *HIE2* distortions with the previously computed error surface: 9 pure flexion-extension trials of the elbow, at 3 different fixed levels of pronation (3 trials at neutral pronation, 3 at complete pronation and 3 at complete supination), 3 trials of prono-supination, at 60° of elbow flexion, and the 4 trials of the “error surface task” of the first group. Each trial required the execution of 4 consecutive cycles of the above specified motions.

Since the subjects executed all movements while keeping the humerus almost completely steady, $H2_{ISG}$ was assumed to provide a reliable estimate of $HIEr$.

2.6 ANALYTICAL DESCRIPTION OF THE ERROR SURFACE AND MEASURES OF PATTERNS SIMILARITY

To obtain the analytical description of the unique error surface for each subject, the 4 trials of the “error surface task” were concatenated and, after a preliminary visual analysis of the data, 3rd and a 5th order polynomial approximations were tested. The quality of fitting was evaluated by computing the Root Mean Square Error ($RMSE$) between the polynomial surface and the experimental data.

To test whether the algorithm that we develop compensated for the $HIE2$ distortions, we evaluated the similarity between $HIEr$ and $HIE2$ patterns before ($HIE2_B$) and after ($HIE2_A$) the application of the algorithm. To quantify the similarity, 4 parameters were computed, which catch different aspects of the similarity relation. The first parameter is the $RMSE$ between the patterns:

$$RMSE = \sqrt{\frac{\sum_{i=1}^{nFrame} e_i^2}{nFrame - 1}} \quad , \quad e_i = HIEr_i - (HIE2_{A,B})_i \quad (5)$$

which can be thought of as a global estimator of the similarity relation. This parameter is optimal when it is equal to 0° (Fig. 5a). The other 3 parameters are related to the linear approximation of the patterns:

$$\begin{cases} HIE2_{A,B} = m \cdot HIEr + q \\ -1 \leq r \leq 1 \end{cases} \quad (6)$$

when they are plotted in the $HIE2$ versus $HIEr$ plane (Fig. 5b); the correlation coefficient r , which quantifies the fraction of $HIEr$ variability explained by $HIE2$ (Petruccelli et al., 1999);

the angular coefficient m , which takes into account the similarity of phase (with its sign) and gain (with its absolute value) of the patterns; and finally the absolute value of q , which takes into account the offset between the patterns. This latter set of 3 parameters is optimal when $r = 1$, $m = 1$ and $q = 0$.

FIGURE 5a,b HERE

3. RESULTS

Regarding the error surface, the 3rd order polynomial approximation gave a *RMSE* of 2.28° on average for the subjects, while the 5th order gave a *RMSE* of 2.23°. Given this small difference and the principle of parsimony (Petruccelli et al., 1999), it seemed reasonable to use a 3rd order approximation to describe \hat{HIE} . This choice was consistent with previous finding obtained *in-vitro* (Cutti et al., 2005b).

Figure 6a-d gives the results for the 4 similarity parameters for each of the task tested, averaged over the trials and the subjects. The sixth column gives the results for the flexion-extension tasks with no distinction between levels of prono-supination, and the seventh column gives the averaged results over the whole set of prono-supination, flexion-extension (using the results from the sixth column), and “error surface” tasks across all subjects.

FIGURE 6a,b,c,d HERE

As can be seen in Figures 6a-b, before application of the algorithm, the patterns of $HIE2_B$ and $HIEr$ ranged from uncorrelated to correlated but were opposite in phase (negative values of m and r), with gain different from 1 and great variability among the subjects. After the application of the algorithm, instead, the patterns of $HIE2_A$ and $HIEr$ were strongly correlated

(r almost equal to 1), in phase, with gain very close to 1, and extremely small degree of patterns variability among the subjects.

As shown in Fig. 6c, there was a general reduction in the offset between the patterns, particularly for the flexion-extension and the error surface tasks, while for the pronosupination task there was a slight increase.

Fig. 6d gives the results for the *RMSE* between the patterns. Based on *RMSE* as a global estimator of the similarity, it can be stated that the application of the algorithm leads to a generalized and substantial reduction in the error due to the kinematic coupling *HIEe*, since the *RMSE* decreased from more than 9° to about 3° , considering the whole set of tasks, with extremely small residual variability among the subjects (0.9°).

4. DISCUSSION

The STA compensation technique proposed here is based on two mainstays: 1) the definition of a humerus bone-embedded frame essentially “artefact free”, but influenced by the orientation of the elbow in the measurement of the humeral axial rotation; 2) the design of an algorithm able to compensate for the kinematic coupling of the new humerus bone-embedded frame and the elbow orientation. In other words, with the compensation technique proposed here, the problem of the STA affecting the estimation of the humeral axial rotation was substituted by the problem of decoupling a humerus bone-embedded frame from the elbow orientation. A key to solving the coupling problem was in estimating, for each subject, the error surface that describes the kinematic coupling; the surface, being invariant with respect to the absolute pose of the humerus, was used to compensate every given trial performed by a subject. Moreover estimation of the error surface was easily obtained by subjects performing only one simple and very short task at the beginning of the motion analysis sessions; this task did not present any particular difficulties for any subject, and thus it can be easily included in a clinical testing session.

The compensation technique is independent of a particular angular convention used to describe the segments orientation; the only requirement is to use the same convention both when computing the error surface and during the compensation in a generic movement trial.

The only limitation of the proposed technique is related to the definition of H2. When the elbow approaches full extension, the orientation of H2 is poorly estimated because the long axes of the humerus and forearm are almost aligned. However, most activities of daily living do not require a fully extended elbow (Buckley et al., 1996), and thus this limitation can be considered minor.

From the results reported here, it appears that the algorithm performs best when compensating for *HIE2* distortion during flexion-extension and error surface trials. Improvement are instead still necessary to obtain such good results also for the pure prono-supination trials. Possible explanations for this behaviour are the small influence of *PS* on *HIE2* compared to *FLEX* (see section 2.1), and the dispersion of the experimental data (*RMSE* of 2.28°) around the approximant error surface. It follows an error surface that is too sensitive to experimental error for accurately modelling the effects of *PS* on *HIE2*. A possible solution to this problem is to use the mean helical axis of prono-supination in the definition of H2, computed applying (Woltring, 2004), instead of the long axis of the forearm as shown in Fig. 1b. The mean helical axis for prono-supination is, by definition, the axis with minimal orientation variation during prono-supination movements; its estimation *in-vivo* was reported to be very stable (Biryukova et al., 2000) and thus it appears to be the optimal axis to minimize the influence of *PS* on *HIE2 a-priori*. Preliminary results, currently under analysis, are confirming this possibility.

To evaluate the ability of the technique to compensate for *HIE2* distortions, we used, as the gold standard, HIE measured by $H2_{ISG}$, assuming that the tasks were executed while the humerus was kept almost completely steady. This choice, even if not optimal, appears to be the only applicable when using an optoelectronic system exclusively.

5. CONCLUSIONS

A new compensation technique for the soft tissue artefact affecting the estimation of the humeral axial rotation was described. Since this technique requires a subject to execute just a simple arm-movement task, it appears to be easily applicable in a clinical setting. Moreover, since the technique does not require any complex, multiple-parameter, non-linear optimisation, it is suitable also for real-time applications. The results provided here indicate the effectiveness of the technique in correcting the soft tissue artefact in most of the tasks that the subjects performed. Additional work is needed for the compensation of the pure pronosupination effects; an explanation for the problem encountered with this task was given and a solution, based on the use of the pronosupination mean helical axis, was proposed to circumvent the problem. Future efforts will be made to test this solution and to further validate the proposed technique using video-fluoroscopy based method.

ACKNOWLEDGMENTS

The authors are grateful to Ing. Gabriele Paolini for his essential aid in managing the acquisitions with the Vicon system, which was kindly provided by I.N.A.I.L.

REFERENCES

- Biryukova, E.V., Roby-Brami, A., Frolov, A.A., Mokhtari, M., 2000. Kinematics of human arm reconstructed from spatial tracking system recordings. *J.Biomech.* 33, 985-995.
- Buckley, M.A., Yardley, A., Johnson, G.R., Carus, D.A., 1996. Dynamics of the upper limb during performance of the tasks of everyday living - a review of the current knowledge base. *Proc.Inst.Mech.Eng [H.]* 210, 241-247.

Cappello, A., Stagni, R., Fantozzi, S., Leardini, A., 2005. Soft tissue artifact compensation in knee kinematics by double anatomical landmark calibration. *IEEE Trans.Biomed.Eng.*: In Press

Cutti, A.G., Paolini, G., Troncossi, M., Cappello, A., Davalli, A., 2005a. Soft tissue artefact assessment in humeral axial rotation. *Gait.Posture.* 21, 341-349.

Cutti, A.G., Cappello, A., and Davalli, A., 2005b. A new technique for compensating the soft tissue artefact at the upper-arm: in vitro validation. *J.Mech.Med.Biology.* 5, 1-15.

Leardini, A., Chiari, L., Croce, U. D., Cappozzo, A., 2005. Human movement analysis using stereophotogrammetry. Part 3. Soft tissue artifact assessment and compensation. *Gait.Posture.* 21, 212-225.

Lucchetti, L., Cappozzo, A., Cappello, A., Della Croce, U., 1998. Skin movement artefact assessment and compensation in the estimation of knee-joint kinematics. *J.Biomech.* 31, 977-984.

Petruccelli, J.D., Nadram, B., Chen, M., 1999. *Applied statistics for engineers and scientists*, first ed. Prentice Hall.

Roux, E., Bouilland, S., Godillon-Maquinghen, A.P., Bouttens, D., 2002. Evaluation of the global optimisation method within the upper limb kinematics analysis. *J.Biomech.* 35, 1279-1283.

Schmidt, R., Disselhorst-Klug, C., Silny, J., Rau, G., 1999. A marker-based measurement procedure for unconstrained wrist and elbow motions. *J.Biomech.* 32, 615-621.

van der Helm, F.C., Makhsous, M., van Roy, P., Anglin, C., Nagels, J., Karduna, A., Veeger, H.E.J., McQuade, K., Wang, X., Chadwick, E., McCormack, B., Nicol, A.C., Peterson, B.,

Waide, V., Werner, F.W., Buchholz, B., 2004. ISB recommendation on definitions of joint coordinate system of various joints for the reporting of human joint motion - Part II: shoulder, elbow, hand and wrist. *J.Biomech.* Submitted.

Veeger, H.E., van der Helm, F.C.T, Rozendal, R.H., 1993. Orientation of the scapula in a simulated wheelchair push. *Clin. Biomech.* 8 (2), 81-90.

Veeger, H.E., Yu, B., An, K.N., Rozendal, R.H., 1997. Parameters for modeling the upper extremity. *J.Biomech.* 30, 647-652.

Wang, X.G., 1996. Construction of arm kinematic linkage from external surface markers. *Proc 4th Int Symp on 3-D analysis of human movement.*

Woltring, H.J., 2004. Data processing and error analysis. In *Biomechanics of human movement*, eds. A. Cappozzo & N. Berme, pp. 203-237. Bertec Corporation, Worthington.

Table 1 Anatomical landmarks used for defining the anatomical reference frames of the thorax, humerus and forearm, following (van der Helm et al., 2004).

Name	Description
<i>PX</i>	Xiphoideus process
<i>IJ</i>	Incisura jugularis
<i>C7</i>	Seventh cervical vertebra
<i>T8</i>	Eighth thoracic vertebra
<i>GH</i>	Glenohumeral joint centre
<i>EL</i>	Lateral epicondyle of the humerus
<i>EM</i>	Medial epicondyle of the humerus
<i>E</i>	$E = (EL + EM)/2$
<i>RS</i>	Radial styloid
<i>US</i>	Ulnar styloid
<i>S</i>	$S = (RS + US)/2$

Table 2 Definition of the anatomical reference frames used, obtained from the ISB recommendations (van der Helm et al., 2004) assuming the ISG preferred orientation for the axes (Z axes pointing backward).

Segment	Axes Definition
Thorax (TH)	$Y_{TH} = (IJ + C7)/2 - (PX + T8)/2 / \ (IJ + C7)/2 - (PX + T8)/2\ $; upward
	$X_{TH} = Y_{TH} \wedge (T8 - PX) / \ Y_{TH} \wedge (T8 - PX)\ $; medio-lateral
	$Z_{TH} = X_{TH} \wedge Y_{TH}$
	Origin = IJ
Upper-Arm (H2 _{ISG})	$Y_{H2} = (GH - E) / \ (GH - E)\ $; longitudinal
	$X_{H2} = Y_{H2} \wedge (E - S) / \ Y_{H2} \wedge (E - S)\ $; medio-lateral
	$Z_{H2} = X_{H2} \wedge Y_{H2}$; antero-posterior
	Origin = GH
	Remark: X _{H2} computed when the elbow is flexed at 90° and in complete pronation (Wang, 1996)
Upper-Arm (H2)	$Y_{H2} = (GH - E) / \ (GH - E)\ $; longitudinal
	$X_{H2} = Y_{H2} \wedge (E - S) / \ Y_{H2} \wedge (E - S)\ $; medio-lateral
	$Z_{H2} = X_{H2} \wedge Y_{H2}$; antero-posterior
	Origin = GH
	Remark: X _{H2} always defined as stated in the formula
Forearm (F)	$Y_F = (E - S) / \ (E - S)\ $; longitudinal
	$Z_F = (RS - US) \wedge Y_F / \ (RS - US) \wedge Y_F\ $; antero-posterior
	$X_F = Y_F \wedge Z_F$; medio-lateral
	Origin = E

Table 2 is part of the on-line material

FIGURE CAPTIONS

Figure 1 – Direction of the axes of the humeral anatomical embedded frames (a) $H2_{ISG}$ and (b) $H2$. $H2_{ISG}$ is defined using a static trial (elbow flexed at 90° and forearm in complete pronation – see also Wang, 1996), through which the position of the humerus and forearm anatomical landmarks is expressed in an arbitrary technical system of reference of the upper-arm cluster; henceforth $H2_{ISG}$ orientation is only linked to this cluster during a dynamic trial. $H2$, for each frame of every trial, is computed from the instantaneous position of the same anatomical landmarks of $H2_{ISG}$, irrespective of elbow orientation. For this reason, $H2$ requires both a forearm and an upper-arm cluster, while $H2_{ISG}$ just requires the upper-arm one. $H2_{ISG}$ definition was obtained from the ISB recommendations (van der Helm et al., 2004), assuming the ISG preferred orientation for the axes (Z axes pointing backward).

Figure 2 – For every frame i of a dynamic trial performed by a subject, the real axial rotation ($HIEr_i$) can be obtained from $HIE2_i$ if the “error surface” is known. The “error surface” describes the error $HIEe_i$ induced on the measurement of the axial rotation by the kinematic coupling of $HIE2$ with the elbow orientation, i.e. by the variation of $FLEX_i$ and PS_i .

Figure 3 – Algorithm scheme of $HIE2$ compensation. ${}^G R_{TH}^i$ represents the orientation of the thorax with respect to a laboratory system of reference. The task of the “Angular decomposition” block is to decompose an orientation matrix into a sequence of angles, such as Euler angles. See text and Table 1 for further details about the symbols.

Figure 4 – Marker locations for upper limb motion analysis. Markers on limb segments are mounted on elastic cuffs to constrain soft tissues. Markers placed on the thorax were located

on *C7*, *T8*, *IJ* and *PX*. The markers on the acromions were used only for 3D model visualisation purposes.

Figure 5 – Example of a flexion-extension trial and the corresponding 4 parameters computed to assess the similarity of *HIE_r* with *HIE2_A* and with *HIE2_B*. (a) *RMSE*, computed in the *HIE versus time* plane; (b) *r*, *m* and *q* computed in the *HIE2 versus HIE_r* plane.

Figure 6 – Results for the different tasks, averaged over the trials and the subjects, before and after the application of the algorithm: “error surface task” (EST), pure prono-supination (PS), pure flexion-extension at neutral pronation (FE1), complete pronation (FE2) and complete supination (FE3). A summary of the results for the flexion-extension tasks is reported in FE, and a summary of results for the entire set of tasks is in ALL. Mean values and standard deviation ± 1 are reported.

Figure 1a,b

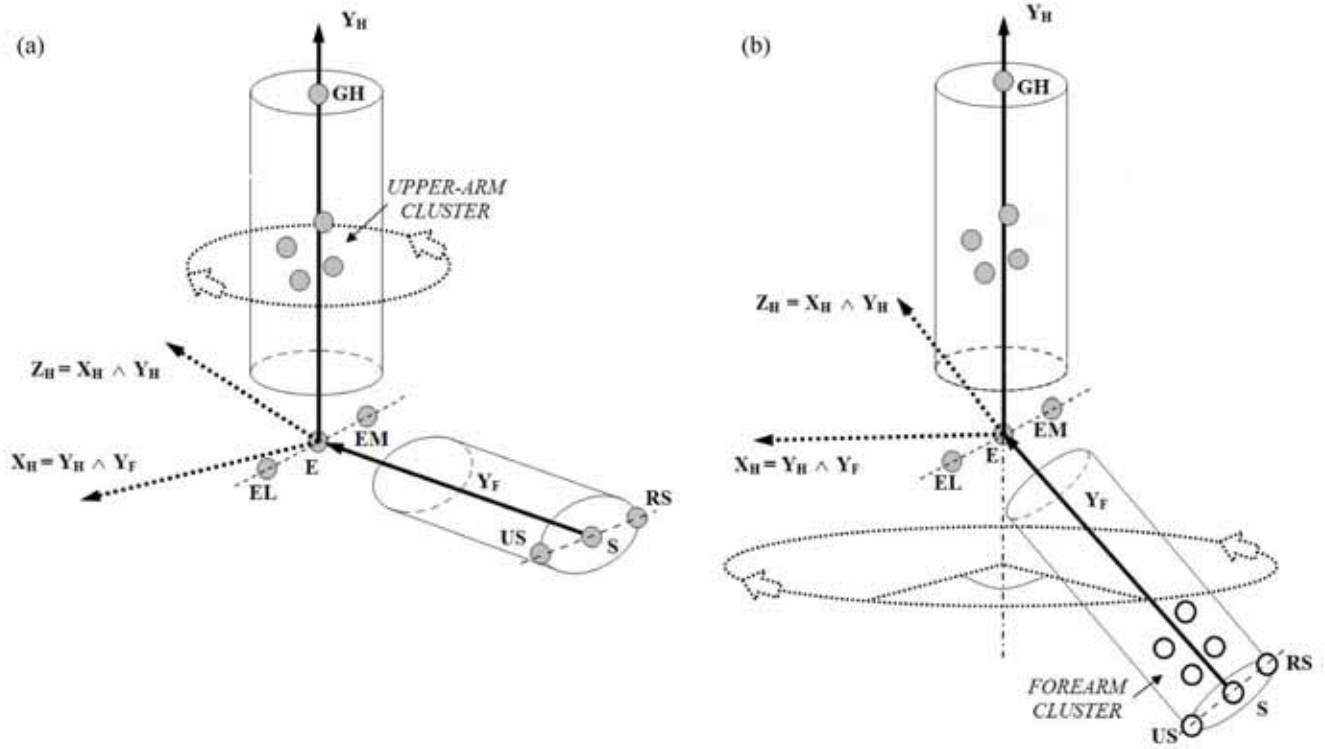


Figure 2 – on-line material

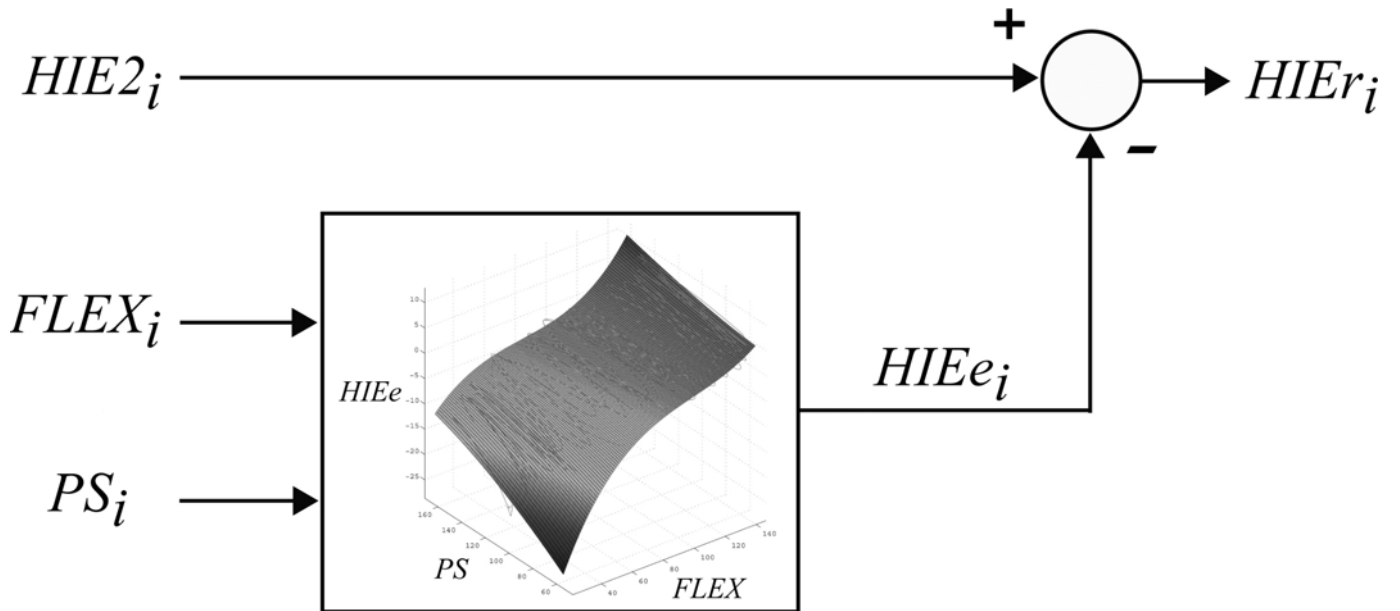


Figure 3 –on-line material.

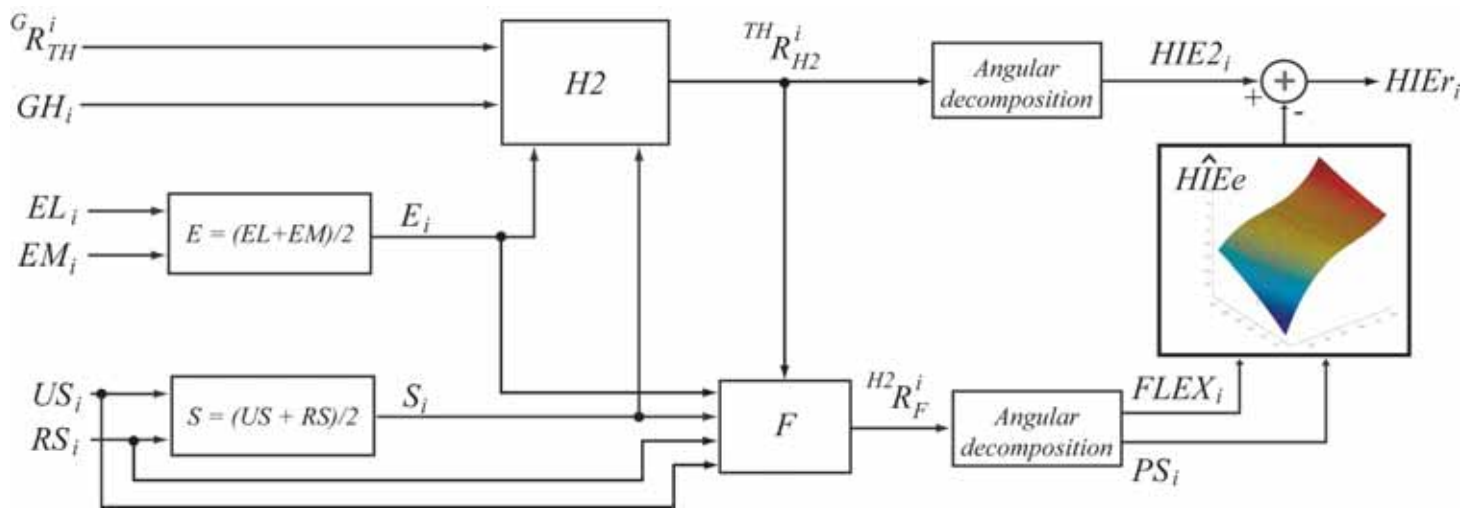


Figure 4 – *on-line material*



Figure 5 a,b

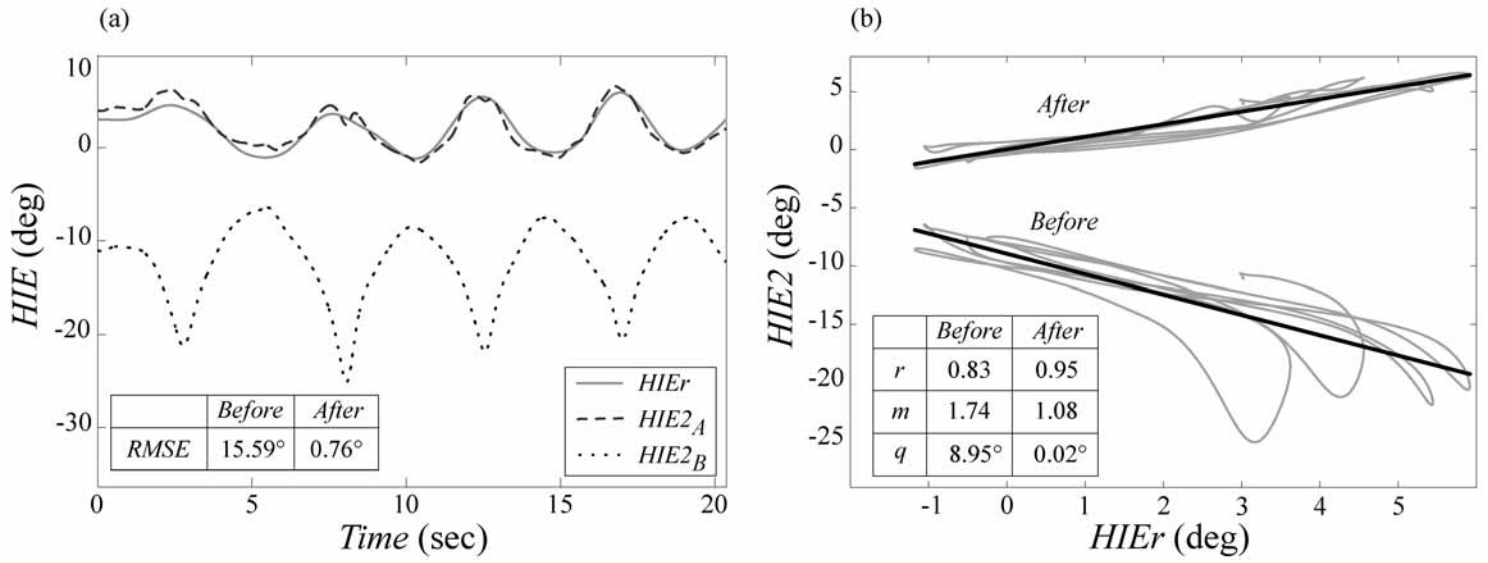


Figure 6 a,b,c,d

